Published in final edited form as:

NMR Biomed. 2011 February ; 24(2): 163–169. doi:10.1002/nbm.1567.

Noninvasive detection of brainstem and spinal cord axonal degeneration in an amyotrophic lateral sclerosis mouse model

Joong Hee Kim[1,*], **Tzy-Haw Wu**[2], **Matthew D. Budde**[3], **Jin-Moo Lee**[4], and **Sheng-Kwei Song**[1]

[1]Department of Radiology, Washington University, St. Louis, MO, USA

[2]Department of Neurology, National Taiwan University Hospital, Taiwan, ROC

[3]Radiology and Imaging Sciences, National Institutes of Health Clinical Center, Bethesda, MD

[4]Department of Neurology, Washington University, St. Louis, MO, USA

Abstract

Degeneration of motor neurons and their associated axons is a hallmark of Amyotrophic Lateral Sclerosis (ALS), but reliable noninvasive modalities to detect this are lacking. In vivo diffusion tensor imaging (DTI) was performed to evaluate neurodegeneration in the brain stem and cervical spinal cord of wild type and G93A-SOD1 transgenic mice, an animal model of ALS. A statistically significant reduction in ADC was observed in motor nuclei VII and XII compared to wild type mice. No significant difference in diffusion anisotropy was observed in dorsal white or gray matter in cervical and lumbar segments of the spinal cord. In contrast, statistically significant decreases in axial diffusivity (the diffusivity parallel to the axis of the spinal cord) and ADC were found in the ventrolateral white matter of G93A-SOD1 mice in both the cervical and lumbar spinal cord. The reduction of axial diffusivity, suggestive of axonal injury, in the white matter of the spinal cord of G93A-SOD1 mice was verified by immunostaining with non-phosphorylated neurofilament. The present study demonstrates that in vivo DTI derived axial diffusivity may be used to accurately evaluate axonal degeneration in an animal model of ALS.

Keywords

Diffusion tensor imaging; Mice; Cervical spinal cord; Axial and radial diffusivity; Diffusion anisotropy; G93A-SOD1; Amyotrophic lateral sclerosis

Introduction

Amyotrophic lateral sclerosis (ALS) is a fatal neurodegenerative disorder characterized by motor neuron degeneration in the cortex, brain stem, and spinal cord (1). Diagnosis of ALS is largely based on clinical history (progressive weakness) and electromyography, which detects signs of upper and lower motor neuron degeneration. Recent observations suggest that there may be several subtypes of ALS distinguished by the differential involvement of

[*]Send correspondence to: Joong Hee Kim, Ph.D., Biomedical MR Laboratory, Campus Box 8227, Washington University School of Medicine, Room 2313, 4525 Scott Ave., St. Louis, MO 63110, USA, Phone: (314) 362-9947, Fax: (314) 362-0526, jhkim@bmr.wustl.edu.

upper vs. upper and lower motor neurons (2). Magnetic resonance spectroscopy (MRS), diffusion MRI, and functional MRI have been used for both clinical and preclinical examinations of ALS revealing tissue alterations induced by neurodegeneration (2–6). However, the specificity of these methods to detect the underlying pathology or to distinguish subtypes has not been established.

SOD1 mutant mice have been widely used for studying ALS. The resemblance in the underlying pathologies of SOD1 transgenic mice to human ALS has resulted in a wide range of studies from fundamental pathogenesis of the disease to its therapeutic intervention. As studies of ALS animal models reveal fundamental mechanisms and potential interventions, a reliable and objective noninvasive diagnostic method is needed. SOD1 mutant mice have been extensively characterized with behavioral phenotypes to evaluate disease progression and efficacy of interventions (1). Although behavioral evaluations permit important functional outcome measures, such characterization does not allow for evaluation of underlying pathophysiology. Recent reports suggest that in vivo diffusion MR measurements can detect disease in the cortex, and brainstem of ALS mice (7–9). However, a systematic and quantitative study of degenerative changes in the brainstem and spinal cord is still lacking. Recent in vivo diffusion tensor imaging of mouse cervical cord has reported highly anisotropic tissue characteristics on white matter with the parallel water diffusion coefficient to be four to six folds of the perpendicular diffusion coefficient (10,11).

In the current study, we employed indices derived from in vivo diffusion tensor imaging (DTI), including fractional anisotropy (FA), axial ($\lambda\|$) diffusivity, radial ($\lambda\perp$) diffusivity, and apparent diffusion coefficient (ADC), to evaluate the progressive degeneration of motor nuclei and axonal tracts in the brainstem and spinal cord in G93A -SOD1 mice. Our results revealed an ADC decrease in brainstem motor nuclei VII and XII, reflecting motor neuron degeneration. Decreased $\lambda\|$ in the ventrolateral white matter of the cervical and lumbar spinal cord was suggestive of axonal degeneration, and this was confirmed with immunohistochemical staining for nonphosphorylated neurofilaments.

Materials and Method

Animal Preparation for Magnetic Resonance Imaging

Twelve week-old female G93A-SOD1 (n = 5) and age-matched wild type mice (n = 5) were employed for in vivo DTI. Animals were anesthetized using isofluorane/oxygen mixture (7% for induction and 0.7 – 1.5% for maintenance). Circulating warm water was used to maintain body temperature at 37 °C. An actively detuned Helmholtz volume coil (6 cm diameter, 10 cm length) was employed for radiofrequency excitation. Two separate actively detuned surface coils were used for imaging either the brainstem and cervical spinal cord or lumbar spinal cord. Both were approximately 1 × 1.5 cm and were tailored to fit the shape of the mouse at each anatomical location. For synchronization of MR data acquisition with animal's respiratory motion, a gated acquisition setup was employed as reported previously (11,12) The entire animal setup was placed in an Oxford Instruments magnet (4.7 T, 40-cm clear bore) equipped with a 10-cm inner diameter, actively shielded Oxford gradient coil capable of producing linear magnetic field gradients up to 60 G/cm having 200 μs rise time. A Varian NMR systems (Palo Alto, CA) INOVA console controlled by a Sun Microsystems

Blade 1500 workstation was used to interface magnet, gradient coil, and gradient power supply.

In Vivo DTI for Brainstem and Spinal Cord

A conventional diffusion spin-echo imaging sequence (13) was used to collect transverse images with respiratory gating. The acquisition parameters were: repetition time (TR) 1.2s (varied according to the respiratory rate), spin echo time (TE) 36ms, time between application of gradient pulses (Δ) 21 ms, diffusion gradient duration (δ) 6 ms, slice thickness 0.5 mm, field of view 1.5 cm × 1.5 cm, data matrix 128 (phase encoding) × 256 (frequency encoding) (zero filled to 256 × 256) producing in-plane resolution 117 μm × 59 μm × 500 μm. Images were obtained with diffusion sensitizing gradients applied in six orientations: (Gx,Gy,Gz) = (E,E,0), (E,0,E), (0,E,E), (E,E,0), (0,E,E), and (E,0,E) where $E = 2^{1/2}$. Two diffusion-sensitizing factors, or b values, were used: 0 and 1.014 ms/μm^2 (1014 s/mm^2). Four scans were averaged per k space line resulting in one hour for full DTI data acquisition for each anatomical location. Following the DTI acquisition of the brainstem and cervical spinal cord, the animal was repositioned inside the magnet and the lumbar spinal cord was imaged at least 24hrs after the initial imaging session.

Data analyses

Using a weighted linear least-squares method (14), diffusion tensors were estimated independently for each pixel from the diffusion-weighted images. Eigen decomposition was applied to the tensor matrix, yielding a set of eigenvalues ($\lambda_1 \geq \lambda_2 \geq \lambda_3$) and eigenvectors for each pixel. Maps of diffusion indices, including ADC, axial diffusivity ($\lambda\|$), radial diffusivity ($\lambda\perp$), and fractional anisotropy (FA), were generated in Matlab (Mathworks, Natick, MA) by applying the following equations for each pixel:

$$\mathrm{ADC} = \langle D \rangle = (\lambda_1 + \lambda_2 + \lambda_3)/3 \quad [1]$$

$$\lambda\| = \lambda_1 \quad [2]$$

$$\lambda\perp = (\lambda_2 + \lambda_3)/2 \quad [3]$$

$$\mathrm{FA} = \frac{\sqrt{3}\sqrt{(\lambda_1 - \langle D \rangle)^2 + (\lambda_2 - \langle D \rangle)^2 + (\lambda_3 - \langle D \rangle)^2}}{\sqrt{2}\sqrt{\lambda_1^2 + \lambda_2^2 + \lambda_3^2}} \quad [4]$$

DTI parameters were quantified using a region of interest (ROI) analysis for nuclei VII and XII, spinal cord dorsal and ventrolateral white matter, and gray matter. A single transverse

image is used for nuclei VII and XII where three and six transverse images were averaged for cervical and lumbar cord.

Histology

Following in vivo DTI, all mice were perfusion fixed through the left ventricle under deep anesthesia with at least 100 ml of 0.1M PBS (pH 7.4) followed by 100 ml of 0.1 M PBS containing 4% paraformaldehyde (pH 7.4). Following fixation, the spine was harvested and placed in fixative (4% paraformaldehyde) for 24 hrs. The C1-2 and lumbar enlargements were excised in 2 mm segments, decalcified with the vertebral column intact, and embedded in paraffin. The embedded tissue was sectioned on a sliding microtome at 5 μm. Immunohistochemistry was performed for non-phosphorylated neurofilament (SMI-32). Briefly, deparaffinized and rehydrated sections were placed in 1 mM EDTA with 95–100°C water bath. After rinsing with 0.01 M PBS and sections were incubated with 0.01 M PBS containing a 2% blocking solution (Invitrogen, Carlsbad, CA) for 1 hour. Sections were then incubated at 4°C overnight with monoclonal anti-SMI32 (1: 5000, Sternberger Monoclonals, Inc., Lutherville, MD) to label non-phosphorylated neurofilament. After rinsing with 0.01 M PBS, sections were incubated with fluorescein isothiocyanate (FITC) – conjugated Fab' fragments (goat anti-mouse or rabbit, 1:300, Jackson ImmunoResearch Laboratories, Inc., West Grove, PA). After washing with PBS, sections were cover-slipped using the Vectashield Mounting Medium with DAPI (Vector Laboratories, CA). Digital images were captured within 1 week following completion of immunohistochemistry. The SMI-32 positive stain were quantified using image J (15) and compared with DTI parameters

Statistics

All statistical analysis was performed with Origin 7.5 SR2 v7.5817 (Origin Lab Co., MA, USA). A Student's t-test was performed to compare DTI parameters between wild type and G93A-SOD1 mice. The correlation between DTI parameters and number of non-phosphorylated neurofilament labeled axons was investigated using Pearson product-moment correlation. Statistical significance was accepted as $p < 0.05$.

Results

The anatomy of the brainstem and cervical and lumbar spinal cord was clearly delineated in T2-weighted images (Fig. 1). In vivo DTI maps provided excellent contrast between gray and white matter, and between brain parenchyma and cerebral spinal fluid (CSF) (Fig. 2). Exploiting this contrast, five regions of interest (ROIs) were manually delineated, including brainstem nuclei VII and XII, spinal cord dorsal white matter, ventrolateral white matter, and gray matter. Differences in ADC between the wild type and G93A-SOD1 were readily apparent in nuclei VII and XII (Fig. 2a and b). FA and $\lambda\perp$ maps of nuclei VII and XII are not shown. Moreover, FA and $\lambda\parallel$ maps showed obvious differences in the ventrolateral white matter of the spinal cord comparing wild type to G93A-SOD1 mice (Fig. 2c and d).

Quantification of DTI parameters from the five ROIs were summarized in Fig. 3. Both nuclei VII and XII exhibited a statistically significant decrease in $\lambda\perp$, $\lambda\parallel$, and ADC, suggestive of significant neurodegeneration, in the absence of changes in FA. In the spinal

cord, dorsal white and gray matter maintained normal DTI parameters, suggesting an intact dorsal column. The ventrolateral white matter showed statistically significant decreases in FA and λ|| in both cervical and lumbar segments of the spinal cord and an approximately 5% increase of λ⊥ in lumbar segment of the cord, suggesting long tract pathology. Interestingly, there were no significant differences in ADC values from all regions of the spinal cord. In good agreement with MRI findings, immunohistochemistry showed dense SMI-32 positive axons in the ventrolateral white matter of G93A -SOD1 transgenic mice (Fig. 4), but not in wild-type mice. Moreover, the dorsal column did not demonstrate evidence of axonal injury with SMI-32. Furthermore, both FA and λ|| showed a statistically significant linear correlation with the density of SMI-32 positive axons, but no significant correlation was seen with either ADC or λ⊥ from both cervical and lumbar cord (Fig. 5).

Discussion

In the current study, we report that in vivo DTI-derived parameters could distinguish neurodegeneration in both gray (nuclei VII and XII in brainstem) and white matter (ventrolateral white matter of spinal cord) in G93A-SOD1 mice. ADC showed selective sensitivity to gray matter neurodegeneration, while diffusion anisotropy (FA) and directional diffusivity (λ||) was sensitive to white matter degeneration. To the best of our knowledge, this is the first in vivo DTI study on mouse cervical cord showing that full tensor derived directional diffusivities (λ|| and λ⊥) could accurately detect neurodegenerative white matter lesion at cervical cord.

ADC changes were used to quantitatively measure the progressive degeneration of nuclei V, VII, and XII in the brainstem of G93A-SOD1 mice, as confirmed by multiple labs (16–18). Recently, the use of quantitative in vivo T2 and ADC measurements to detect neurodegeneration in G93A-SOD1 mice was expanded from brainstem to cervical cord (8). T2 alterations were seen in brain stem nuclei and cervical cord, whereas ADC decreases were seen in brainstem nuclei but not in cervical cord. This may suggest that spin-spin relaxation (T2) may have high sensitivity to motor neuron integrity in mouse spinal cord. Previous histological analysis has demonstrated motor neuron degeneration in the spinal cord of G93A-SOD1 mice (19,20). To determine whether the full tensor analysis more accurately reflects this underlying pathology, DTI derived parameters (FA, λ||, and λ⊥) of brain stem and spinal cord were examined in the present study. Our findings are consistent with those by Nissen et al. demonstrating alterations of ADC in brainstem but not in the whole spinal cord (combining both gray and white matter) (Fig. 3). In the gray matter of spinal cord, none of the measured DTI parameters showed a significant difference between G93A-SOD1 and wild type mice (Fig. 3). In contrast, statistically significant changes in the DTI parameters between G93A-SOD1 and wild type mice were observed in the spinal cord white matter (Fig. 3), and these changes were validated with histological evaluation (Fig. 4).

We have previously found that both λ|| and λ⊥ can detect axon and myelin pathology, respectively, in the mouse brain (21,22). The use of λ|| as a biomarker of axonal injury in spinal cord has recently been reported in mouse models of multiple sclerosis (12,23) and traumatic spinal cord injury (Kim et al., 2007; Loy et al., 2007) with histological validation. In addition, ex vivo measurements of directional diffusivity correlated well with histological

measures of axon and myelin integrity (24,25). Despite the controversy over whether G93A-SOD1 accurately reflects human ALS, the motor neuron degeneration observed in G93A-SOD1 mice is clearly evident as seen in numerous studies. It is widely believed that motor neuron degeneration is accompanied by secondary axonal degeneration in the spinal cord. This is consistent with our observed decrease in $\lambda\|$ in the ventrolateral white matter of cervical and lumbar segments of the spinal cord from G93A-SOD1 mice ($p < 0.001$) (Fig 3). This signature of axonal injury was confirmed by positive SMI-32 staining in the ventrolateral white matter of spinal cords from G93A-SOD1 mice (Fig. 4). Similar corticospinal tract degeneration has been observed in post-mortem analysis in spinal cords of ALS patients (26). The significant linear correlation between $\lambda\|$ and SMI-32 positive axonal counts at ventrolateral white matter of cervical and lumbar cord further quantitatively support the potential of $\lambda\|$ as biomarker for axon degeneration in the spinal cord of ALS patients (Fig. 5). Our finding suggests that neurodegeneration may reach beyond the cervical spinal cord and the selective loss of axon fibers in the spinal cord from G93A-SOD1mice.

In addition to selective sensitivity of DTI parameters to neurodegeneration in G93A-SOD1 mice, the differential changes in DTI parameters were selective for gray vs. white matter. Both directional diffusivities ($\lambda\|$ and $\lambda\perp$) in nuclei VII and XII of the brainstem from G93A-SOD1 mice decreased compared with those of control mice. The statistically significant reduction of both $\lambda\|$ and $\lambda\perp$ resulted in a cumulative effect on ADC values. However, there was no change in FA between wild type and G93A-SOD1 mice. In the ventrolateral white matter of G93A-SOD1 mouse spinal cord, $\lambda\|$ significantly decreased with a minimal (~8%) increase in $\lambda\perp$ compared to wild type mice. This also resulted in a statistically significant FA reduction. The correlation between FA and $\lambda\|$ with the number of SMI-31 positive axons supports the notion that $\lambda\|$ may be a potential biomarker of axon injury in spinal cords of ALS mice and patients.

In conclusion, the current results suggest that in vivo DTI may be used to monitor the progression of neurodegeneration in ALS separately in the brainstem and spinal cord, and this may help to distinguish between ALS subtypes. Among the two widely used diffusion indices, FA and ADC, the presented results suggest FA is sensitive to axonal degeneration in white matter and ADC is sensitive to neuron degeneration in gray matter. As new treatments are developed using G93A-SOD1 mice as a preclinical model, in vivo DTI combined with conventional T1 and T2 MRI measurements could be more effective in quantifying the underlying disease progression and treatment efficiency.

Acknowledgments

Grant information: This study was supported in part by the National Multiple Sclerosis Society (RG 3376-A-2/1, and CA 1012-A-13), NIH (R01-NS054194, R01-NS047592, R01 NS048283, P01 NS032636), University of Missouri Spinal Cord Injuries Program, and the Washington University Small Animal Imaging Resource (WUSAIR) (NIH: R24-CA83060), and the Animal Models Core of the Hope Center for Neurological Disorders.

This study was supported in part by the National Multiple Sclerosis Society (RG 3376-A-2/1, and CA 1012-A-13), NIH (R01-NS047592, R01 NS048283, P01 NS032636), University of Missouri Spinal Cord Injuries Program, and the Washington University Small Animal Imaging Resource (WUSAIR) (NIH: R24-CA83060), and the Animal Models Core of the Hope Center for Neurological Disorders.

References

1. Weydt P, Hong SY, Kliot M, Moller T. Assessing disease onset and progression in the SOD1 mouse model of ALS. Neuroreport. 2003; 14:1051–1054. [PubMed: 12802201]
2. Ellis CM, Simmons A, Jones DK, Bland J, Dawson JM, Horsfield MA, Williams SC, Leigh PN. Diffusion tensor MRI assesses corticospinal tract damage in ALS. Neurology. 1999; 53:1051–1058. [PubMed: 10496265]
3. Wang S, Melhem ER. Amyotrophic lateral sclerosis and primary lateral sclerosis: The role of diffusion tensor imaging and other advanced MR-based techniques as objective upper motor neuron markers. Ann N Y Acad Sci. 2005; 1064:61–77. [PubMed: 16394148]
4. Pioro EP. Proton magnetic resonance spectroscopy (1H-MRS) in ALS. Amyotroph Lateral Scler Other Motor Neuron Disord. 2000; 1(Suppl 2):S7–16. [PubMed: 11464945]
5. Brooks BR, Bushara K, Khan A, Hershberger J, Wheat JO, Belden D, Henningsen H. Functional magnetic resonance imaging (fMRI) clinical studies in ALS--paradigms, problems and promises. Amyotroph Lateral Scler Other Motor Neuron Disord. 2000; 1(Suppl 2):S23–32. [PubMed: 11464937]
6. Pagani E, Horsfield MA, Rocca MA, Filippi M. Assessing atrophy of the major white matter fiber bundles of the brain from diffusion tensor MRI data. Magn Reson Med. 2007; 58:527–534. [PubMed: 17763353]
7. Angenstein F, Niessen HG, Goldschmidt J, Vielhaber S, Ludolph AC, Scheich H. Age-dependent changes in MRI of motor brain stem nuclei in a mouse model of ALS. Neuroreport. 2004; 15:2271–2274. [PubMed: 15371748]
8. Niessen HG, Angenstein F, Sander K, Kunz WS, Teuchert M, Ludolph AC, Heinze HJ, Scheich H, Vielhaber S. In vivo quantification of spinal and bulbar motor neuron degeneration in the G93A-SOD1 transgenic mouse model of ALS by T2 relaxation time and apparent diffusion coefficient. Exp Neurol. 2006; 201:293–300. [PubMed: 16740261]
9. Wilson JM, Petrik MS, Grant SC, Blackband SJ, Lai J, Shaw CA. Quantitative measurement of neurodegeneration in an ALS-PDC model using MR microscopy. Neuroimage. 2004; 23:336–343. [PubMed: 15325381]
10. Callot V, Duhamel G, Cozzone PJ, Kober F. Short-scan-time multi-slice diffusion MRI of the mouse cervical spinal cord using echo planar imaging. NMR Biomed. 2008; 21:868–877. [PubMed: 18574855]
11. Kim JH, Haldar J, Liang ZP, Song SK. Diffusion tensor imaging of mouse brain stem and cervical spinal cord. J Neurosci Methods. 2009; 176:186–191. [PubMed: 18834905]
12. Kim JH, Budde MD, Liang HF, Klein RS, Russell JH, Cross AH, Song SK. Detecting axon damage in spinal cord from a mouse model of multiple sclerosis. Neurobiol Dis. 2006; 21:626–632. [PubMed: 16298135]
13. Stejskal ET, JE. Spin Echoes in the Presence of a Time-Dependent Field Gradient. The Journal of Chemical Physics. 1965; 42(1):288–292.
14. Koay CG, Chang LC, Carew JD, Pierpaoli C, Basser PJ. A unifying theoretical and algorithmic framework for least squares methods of estimation in diffusion tensor imaging. J Magn Reson. 2006; 182:115–125. [PubMed: 16828568]
15. Rasband, WS. ImageJ. U.S. National Institutes of Health; Bethesda, MD: 1997–2005.
16. Gurney ME. What transgenic mice tell us about neurodegenerative disease. Bioessays. 2000; 22:297–304. [PubMed: 10684590]
17. Ralph GS, Radcliffe PA, Day DM, Carthy JM, Leroux MA, Lee DC, Wong LF, Bilsland LG, Greensmith L, Kingsman SM, Mitrophanous KA, Mazarakis ND, Azzouz M. Silencing mutant SOD1 using RNAi protects against neurodegeneration and extends survival in an ALS model. Nat Med. 2005; 11:429–433. [PubMed: 15768029]
18. Zang DW, Yang Q, Wang HX, Egan G, Lopes EC, Cheema SS. Magnetic resonance imaging reveals neuronal degeneration in the brainstem of the superoxide dismutase 1 transgenic mouse model of amyotrophic lateral sclerosis. Eur J Neurosci. 2004; 20:1745–1751. [PubMed: 15379995]

19. Gurney ME, Pu H, Chiu AY, Dal Canto MC, Polchow CY, Alexander DD, Caliendo J, Hentati A, Kwon YW, Deng HX, et al. Motor neuron degeneration in mice that express a human Cu,Zn superoxide dismutase mutation. Science. 1994; 264:1772–1775. [PubMed: 8209258]
20. Wong PC, Pardo CA, Borchelt DR, Lee MK, Copeland NG, Jenkins NA, Sisodia SS, Cleveland DW, Price DL. An adverse property of a familial ALS-linked SOD1 mutation causes motor neuron disease characterized by vacuolar degeneration of mitochondria. Neuron. 1995; 14:1105–1116. [PubMed: 7605627]
21. Song SK, Sun SW, Ju WK, Lin SJ, Cross AH, Neufeld AH. Diffusion tensor imaging detects and differentiates axon and myelin degeneration in mouse optic nerve after retinal ischemia. Neuroimage. 2003; 20:1714–1722. [PubMed: 14642481]
22. Song SK, Sun SW, Ramsbottom MJ, Chang C, Russell J, Cross AH. Dysmyelination revealed through MRI as increased radial (but unchanged axial) diffusion of water. Neuroimage. 2002; 17:1429–1436. [PubMed: 12414282]
23. Budde MD, Kim JH, Liang HF, Russell JH, Cross AH, Song SK. Axonal injury detected by in vivo diffusion tensor imaging correlates with neurological disability in a mouse model of multiple sclerosis. NMR Biomed. 2008; 21:589–597. [PubMed: 18041806]
24. Schwartz ED, Cooper ET, Chin CL, Wehrli S, Tessler A, Hackney DB. Ex vivo evaluation of ADC values within spinal cord white matter tracts. AJNR Am J Neuroradiol. 2005; 26:390–397. [PubMed: 15709142]
25. Schwartz ED, Hackney DB. Diffusion-weighted MRI and the evaluation of spinal cord axonal integrity following injury and treatment. Exp Neurol. 2003; 184:570–589. [PubMed: 14769351]
26. Ravits J, Laurie P, Fan Y, Moore DH. Implications of ALS focality: rostral-caudal distribution of lower motor neuron loss postmortem. Neurology. 2007; 68:1576–1582. [PubMed: 17485644]

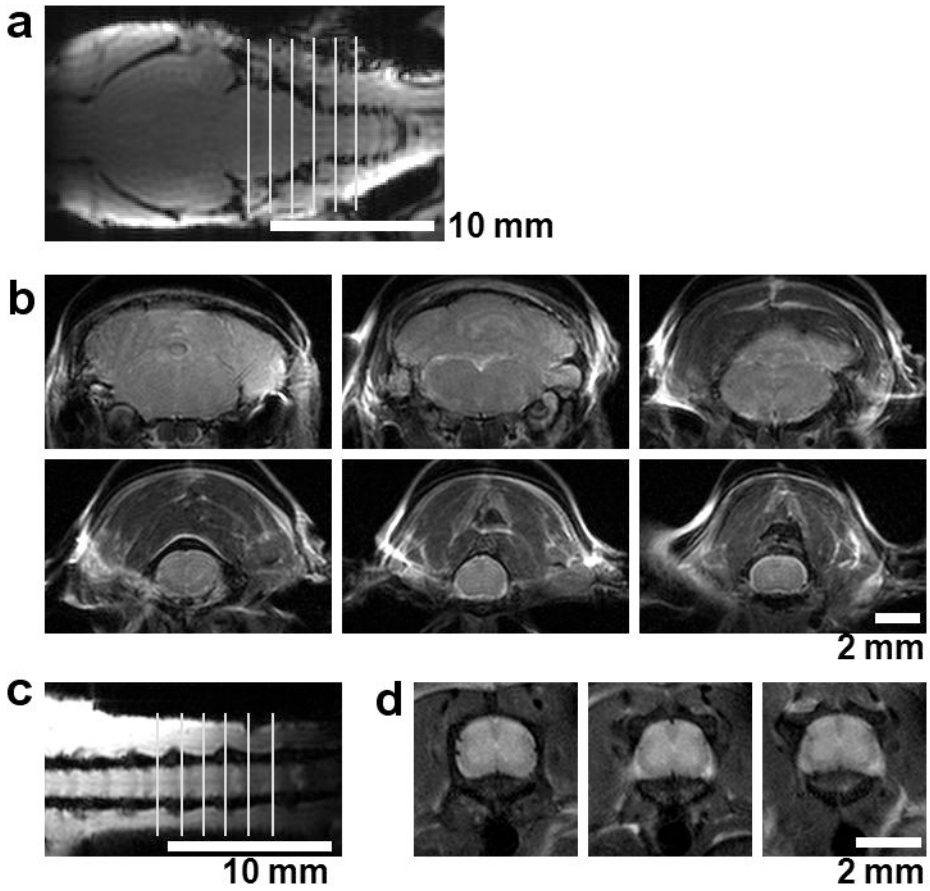

Figure 1.

Anatomical MR images of mouse brain and spinal cord. Transverse (a, c) and coronal (b, d) images of the brain and spinal cord are shown clearly demonstrating the anatomy of the brainstem (b, upper panel), cervical cord (b lower panel), and lumbar cord (d). Each image is 0.5 mm thick with a 1.0 mm gap between images.

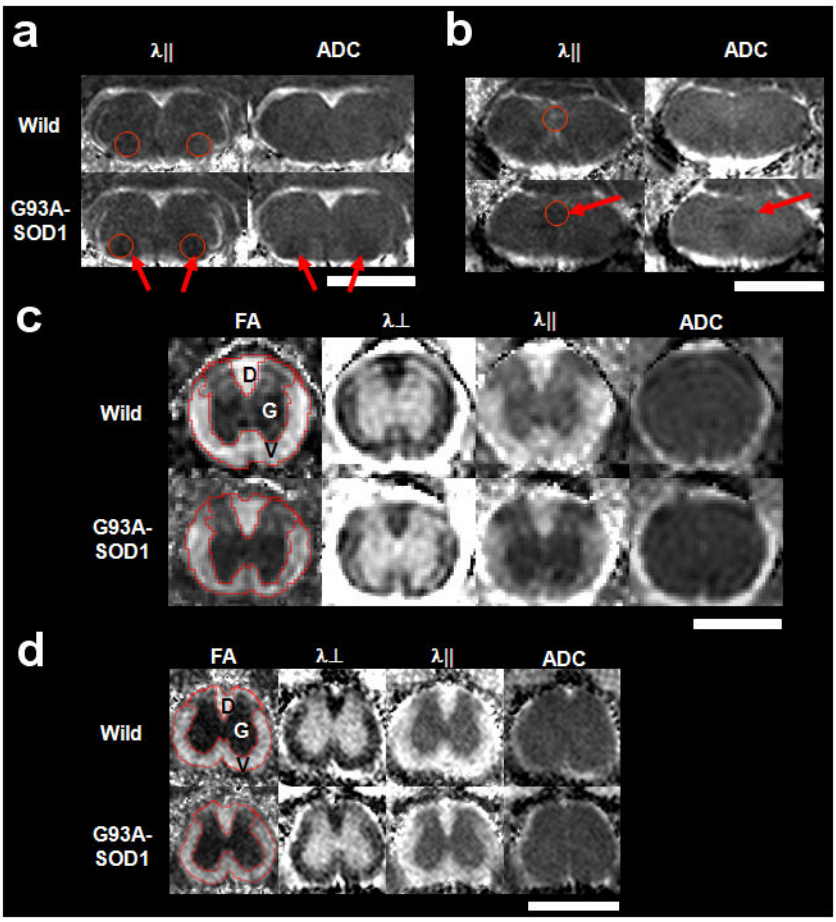

Figure 2.

The *in vivo* diffusion tensor parameter maps of wild type and G93A-SOD1 mice are shown for brainstem (a & b), cervical (c), and lumbar spinal cord (d). Nuclei VII (a, circles) and XII (b, circles) in the brainstem show distinct differences between wild type and G93A-SOD1 mice in axial (λ||) and ADC indicated by the arrows. In both cervical (c) and lumbar (d) spinal cord, the difference between wild type and G93A-SOD1 mice is seen in FA and λ|| maps in the ventrolateral white matter (V), but not in dorsal white matter (D) or gray matter (G). Image scales are as follows: FA, 0.0 – 1.0 (unitless); λ⊥, 0.0 – 1.0 μm^2/ms; λ||, 0.0 – 3.0 μm^2/ms; and ADC, 0.0 – 1.0 μm^2/ms. The white bars represent 2.0 mm

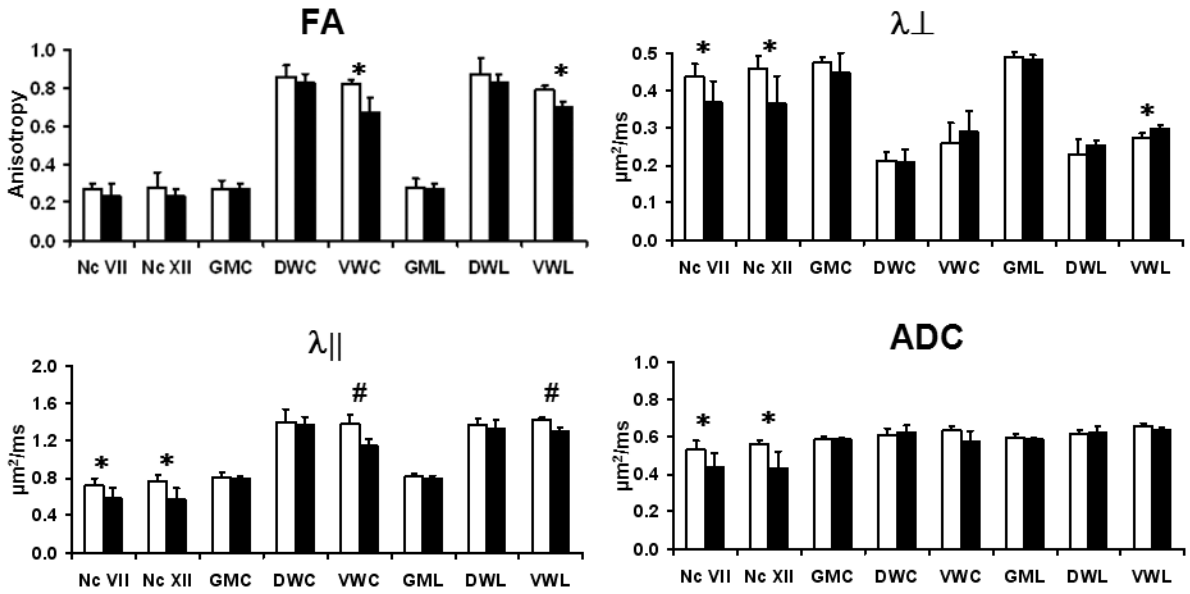

Figure 3.

The quantified DTI parameters from brainstem and spinal cord of wild type (white) and G93A-SOD1 (black) are shown with mean ± standard deviation (n = 5 for each group). Compared to wild type, G93A-SOD1 mice show statistically significant differences in λ||, λ⊥, and ADC in both Nc VII and Nc XII. The ventrolateral white matter of cervical and lumbar cord shows significant differences in λ|| and RA map. Nc VII – brainstem nuclei VII, Nc XII – brainstem nuclei XII, GMC – cervical gray matter, DWC – cervical dorsal white matter, VWC - cervical ventrolateral white matter GML – lumbar gray matter, DWL – lumbar dorsal white matter, and VWL – lumbar ventrolateral white matter. * - $p < 0.05$; # - $p < 0.001$.

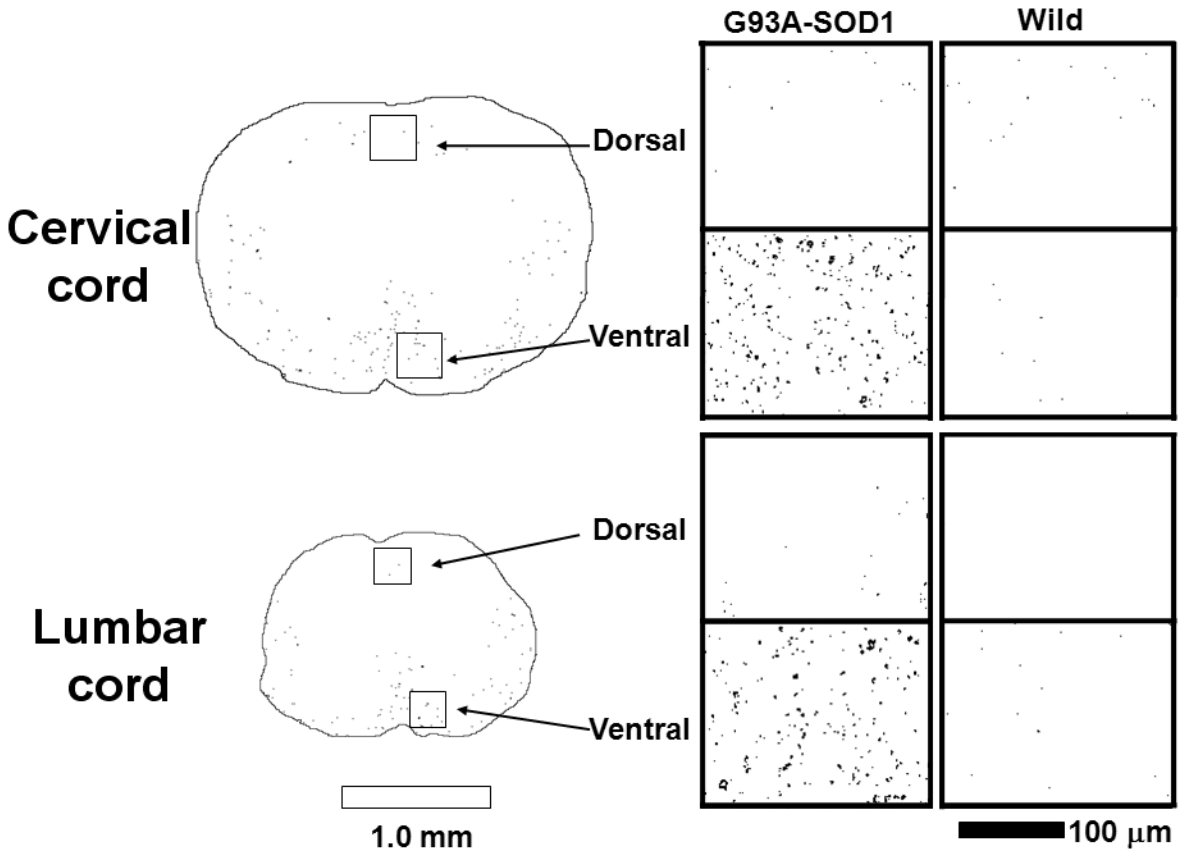

Figure 4.

Histopathological sections from spinal cord white matter stained for SMI-32, non-phosphorylated neurofilaments. For both cervical and lumbar cord, G93A-SOD1 mice have significantly more SMI-32 positive axons in ventrolateral white matter compared to wild type mice. In contrast, there is no discernable difference in SMI-32 staining in dorsal white matter for either the cervical or lumbar white matter. White and black bar represents 1.0 mm and 100 μm each.

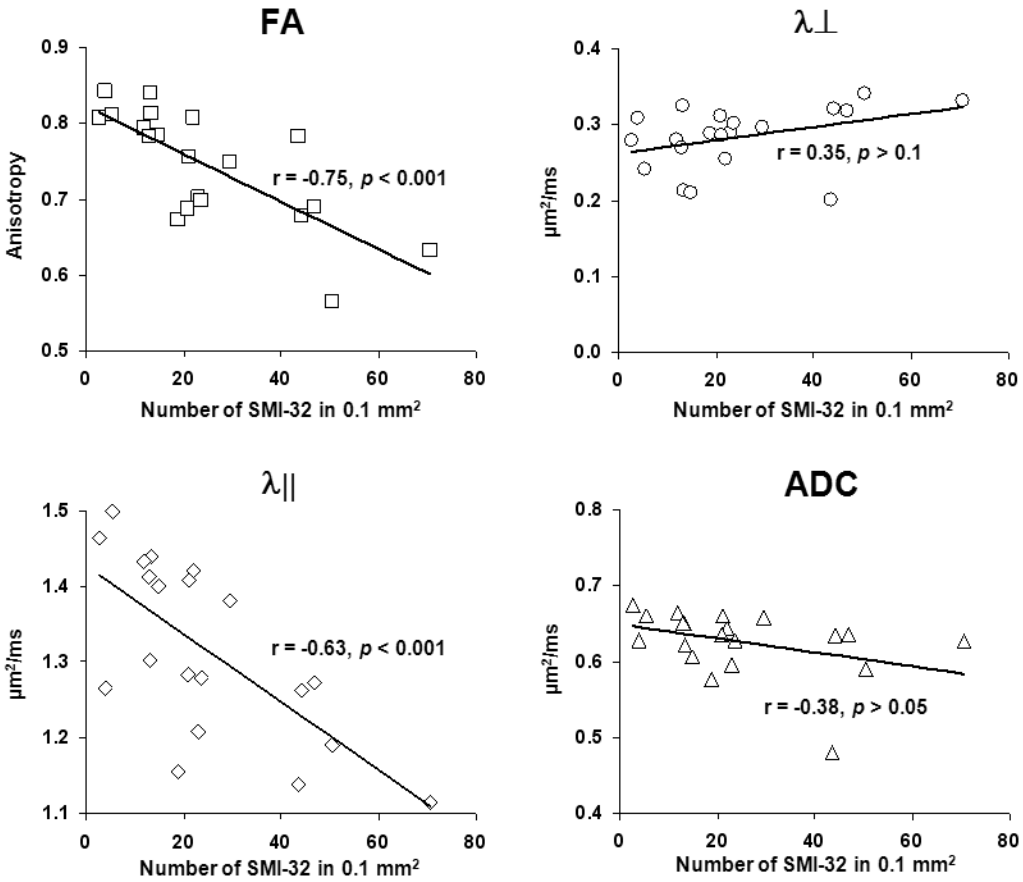

Figure 5.

Correlations between DTI parameters and SMI-32 staining density from ventrolateral white matter of cervical, and lumbar cord. Both λ|| and RA show significant negative correlations with SMI-32 density, reflecting their association with axonal damage. In contrast, λ⊥ and ADC were not significantly correlated with SMI-32.